interesting to note that the $M_{4n+6}Ge_{2n+1}O_{8(n+1)}$ series is intermediate between olivine and spinel in terms of density of atom packing: in the $MgO-GeO_2$ system, the structures of $Mg_2GeO_4$ spinel, $Mg_{14}Ge_5O_{24}$ and $Mg_2GeO_4$ olivine correspond to volumes of 17·58, 18·36 and 19·04 Å$^3$ per O atom respectively [values based on data from Von Dreele *et al.* (1970) and Navrotsky (1973)].

Because germanates are usually regarded as lower-pressure analogues of silicates (*e.g.* Ringwood, 1975), the existence of the $(Ni,Mg)_{4n+6}Ge_{2n+1}O_{8(n+1)}$ series at atmospheric pressure suggests that a similar structural family may exist at high pressure in silicate systems such as $MgO-SiO_2$. In that respect, it is interesting to point out that in their investigation by electron microscopy of the olivine → spinel transition in $Mg_2SiO_4$, Boland & Liu (1983) observed olivine crystals heavily faulted on (001) planes (for the *Pnma* setting of the olivine unit cell). Although these faults, observed at low magnification, have been associated with the olivine → $\Omega$-phase transition [the $\Omega$-phase being the 'linking' spinelloid phase – *cf.* Hyde *et al.* (1982)], the same type of faults would also be expected from disordered (001) intergrowths of thin slabs of phases from the $Mg_{4n+6}Si_{2n+1}O_{8(n+1)}$ series (*cf.* Figs. 7–11). It appears that high-resolution electron microscopy would be required in order to distinguish between, in particular, images of thin slabs of the two linking $M1$ and $\Omega$ structures: both correspond to a cubic close-packing of O atoms but, whereas the $\Omega$-phase contains olivine-type layers only (Hyde *et al.*, 1982), the $M1$ phase is a 1 : 1 intergrowth of olivine and rock-salt layers. The only difference between the two structures therefore resides in the cation content and distribution within half of the cubic close-packed layers. Finally, it may be noted that the cation distribution in the structures of the hypothetical $Mg_{4n+6}Si_{2n+1}O_{8(n+1)}$ series would require some Si atoms to be six-coordinated within the d rock-salt layers. Although this condition suggests that these structures could only be stable at relatively high pressures, it may not be prohibitive as very high pressures are indeed involved in these transformations [*e.g.* 220 kbar (22 GPa) in Boland & Liu's experiment].

### References


AKAOGI, M., AKIMOTO, S. HORIOKA, S., TAKAHASHI, K. & HORIUCHI, H. (1982). *J. Solid State Chem.* **44**, 257–267.

BARBIER, J. (1987). *J. Solid State Chem.* **67**, 52–60.

BARBIER, J. & HYDE, B. G. (1986). *Phys. Chem. Miner.* **13**, 382–392.

BOLAND, J. N. & LIU, L. G. (1983). *Nature (London)*, **303**, 233–235.

CHRIST, C. L. & CLARK, J. R. (1955). *Am. Mineral.* **40**, 907–916.

DACHILLE, F. & ROY, R. (1960). *Am. J. Sci.* **258**, 225–246.

DAVIES, P. K. & NAVROTSKY, A. (1983). *J. Solid State Chem.* **46**, 1–22.

HAMAYA, N. & AKIMOTO, S. (1982). *Phys. Earth Planet. Inter.* **29**, 6–11.

HYDE, B. G., WHITE, T. J., O'KEEFFE, M. & JOHNSON, A. W. S. (1982). *Z. Kristallogr.* **160**, 53–62.

MA, C. B. (1974). *Contrib. Mineral. Petrol.* **45**, 257–279.

MADON, M. & POIRIER, J. P. (1983). *Phys. Earth Planet. Inter.* **33**, 31–44.

MARUMO, F., ISOBE, M. & AKIMOTO, S. (1977). *Acta Cryst.* B**33**, 713–716.

MORIMOTO, N., TOKONAMI, M., WATANABE, M. & KOTO, K. (1974). *Am. Mineral.* **59**, 475–485.

NAVROTSKY, A. (1973). *J. Solid State Chem.* **6**, 21–41.

ROBBINS, C. R. & LEVIN, E. M. (1959). *Am. J. Sci.* **257**, 63–70.

RINGWOOD, A. E. (1961). *Aust. J. Sci.* pp. 378–379.

RINGWOOD, A. E. (1975). In *Composition and Petrology of the Earth's Mantle*. New York: McGraw-Hill.

VON DREELE, R. B., BLESS, P. W., KOSTINER, E. & HUGHES, R. E. (1970). *J. Solid State Chem.* **2**, 612–618.

WYCKOFF, R. W. G. (1965). In *Crystal Structures*, 2nd ed. New York: Interscience.


*Acta Cryst.* (1987). B**43**, 429–434

# $K_x(Nb,W)_{17}O_{47}$ ($1 \le x \le 2$): a New Tunnel Structure Derived from High-Resolution Electron Micrographs


BY MARGARETA SUNDBERG AND MONICA LUNDBERG

*Department of Inorganic Chemistry, Arrhenius Laboratory, University of Stockholm, S-106 91 Stockholm, Sweden*


(*Received* 19 *January* 1987; *accepted* 18 *May* 1987)


## Abstract

A new tunnel structure of a fully oxidized compound with the general formula $K_xNb_{8+x}W_{9-x}O_{47}$ ($1 \le x \le 2$) has been deduced from high-resolution electron micrographs. For $x = 2$ the monoclinic unit-cell parameters are $a = 18{\cdot}882\,(5)$, $b = 3{\cdot}9572\,(5)$, $c = 12{\cdot}378\,(2)$ Å, $\beta = 102{\cdot}93\,(3)°$, $V = 901{\cdot}41$ Å$^3$, $Z = 1$, $M_r = 3046{\cdot}2$ and $D_x = 5{\cdot}61$ g cm$^{-3}$. The space group is $P2/m$. The structure has been confirmed by simulated image calculations and by X-ray powder diffraction studies. The polyhedral framework is built up of octahedra and pentagonal columns in such a way that four-, five- and six-sided tunnels are formed. The structure comprises features of both the $W_{18}O_{49}$ and the tetragonal tungsten bronze (TTB) structure types.


0108-7681/87/050429-06$01.50

Phases obtained for values of $x = 3$ and 5 possess structures of the $Nb_8W_9O_{47}$ type. Intergrowth between the tunnel structure reported here and the latter TTB-type structure has also been observed.

## Introduction

The K–Nb–O and K–Nb–O–F systems include a variety of phases. Some of these have recently been characterized by X-ray powder diffraction and high-resolution electron microscopy (HREM) techniques (Lundberg & Sundberg, 1986, and references therein; Li, Lundberg, Werner & Westdahl, 1984; Sundberg & Lundberg, 1987).

Lately our interest has been focused on phases with low potassium content. In order to examine the existence of similar phases containing the same transition metal to potassium ratio our study was extended to comprise a few oxide compounds with $Nb^V$ partly replaced by $W^{VI}$.

During our experiments one specimen with the gross composition $KNb_3W_4O_{20}$ was found to consist of two phases: a hexagonal tungsten bronzoid (HTB) type and a new compound. The structure of this new phase has been deduced from HREM micrographs, and it will be discussed in terms of structural building units recognized in related compounds. The transition-metal–oxygen composition is $M_{17}O_{47}$, but it is neither the $Nb_8W_9O_{47}$ (Sleight, 1966) nor the $Mo_{17}O_{47}$ (Kihlborg, 1960) structure type.

## Experimental

Samples of compositions $KNb_3W_4O_{20}$ and $K_xNb_{8+x}W_{9-x}O_{47}$ ($x = 1, 2, 3$ and 5) were obtained by heating appropriate amounts of $KNbO_3$ [prepared as described by Lundberg & Sundberg (1986)], $Nb_2O_5$ (Merck, optipure, purified of oxide fluorides in air at 1375 K) and $WO_3$ (Johnson Matthey Chemicals, specpure) in sealed platinum tubes at 1350 K for five days. The products were colourless and microcrystalline. The unit-cell dimensions were derived from an X-ray powder pattern, recorded in a Guinier-Hägg type diffraction camera, and refined with the least-squares program *PIRUM* (Werner, 1969).

Electron-microscope specimens were prepared by crushing a small amount of the sample in an agate mortar and then dispersing it in *n*-butanol. A drop of the resultant suspension was allowed to dry on a perforated carbon film supported on a Cu grid. The grid was then studied in a Jeol 200CX electron microscope operated at 200 kV and equipped with an ultra-high-resolution top-entry goniometer stage with tilt angles of $\pm 10°$. HREM images were recorded of thin fragments aligned with a short axis parallel to the electron beam. The objective aperture used corresponded to 0·41 $Å^{-1}$ in reciprocal space. Simulated images were calculated according to the multislice method, using locally modified versions of the *SHRLI* suite of programs (O'Keefe, Buseck & Iijima, 1978).

## Results and discussion

The electron diffraction study of thin crystal fragments from the $KNb_3W_4O_{20}$ specimen showed that mainly two phases were present: an HTB-related phase, $K_xNb_xW_{1-x}O_3$ (Deschanvres, Frey, Raveau & Thomazeau, 1968), and a second phase that could not be assigned any known structure. The latter phase had a unit cell of monoclinic symmetry with approximate parameters $a = 18·9$, $b = 3·95$, $c = 12·4$ Å, $\beta = 102·5°$ as observed in the electron diffraction patterns. The length of the $c$ axis (~12·4 Å) is of the same order as that reported for the tetragonal tungsten bronze (TTB) type structures (12·2–12·6 Å). A few recorded electron diffraction patterns showed intergrowth between the new phase and a phase with a basic structure of TTB type but with a tripled unit cell, *i.e.* the $Nb_8W_9O_{47}$ structure type denoted 3-TTB below.

A crystal structure image recorded of a thin fragment of the new phase is shown in Fig. 1(*a*). The black contrast features change with increasing thickness. A structure model was deduced from the pattern of black spots observed in the thinnest part at the edge of the crystal flake; it is shown in Fig. 1(*b*). The unit cell is outlined, and the polyhedral framework corresponds to the stoichiometry $M_{17}O_{47}$. In the model, there is one six-sided, two five-sided and four four-sided tunnels available per unit cell in which the potassium required for electroneutrality can be located. The sample examined was colourless, which suggests that it is a fully oxidized compound. This leads to the general formula $K_xNb_{8+x}W_{9-x}O_{47}$, with $x_{max} = 7$, if all the above-mentioned tunnels are occupied by potassium.

Approximate atomic coordinates (Table 1) were derived from the structure model in Fig. 1(*b*). Reasonable positions for the O atoms were found by calculations of interatomic distances. A set of HREM images were simulated for this model with two K atoms located in the five-sided tunnels, corresponding to the formula $K_2Nb_{10}W_7O_{47}$. Some of these images are shown in Fig. 2. There is rather good agreement between the image of the thinnest part of the flake (Fig. 1*a*) and that calculated for a crystal thickness of 19·8 Å and a defocus value of −460 Å (Fig. 2*c*). However, the K atoms in the five-sided tunnels give rise to a weak contrast feature in the calculated image which is less distinguishable in the HREM image. This might indicate that the examined fragment does not have full occupancy of potassium in the five-sided tunnels. As can be seen from Fig. 2, there is a region (defocus values of −420 to −480 Å) where the five-sided tunnels appear almost empty. Without a rather precise knowledge of the defocus and the thickness,

it does not seem possible to determine the location or the amount of potassium present in the examined fragment from HREM micrographs. This is in agreement with previous results obtained for the H-$KNb_3O_8$ compound (Lundberg & Sundberg, 1986).

According to the X-ray diffraction pattern the specimen of gross composition $KNb_3W_4O_{20}$ consisted mainly of an HTB-related compound. However, some lines could not be indexed on the basis of an HTB cell. We assumed that these lines belonged to the phase observed by HREM. In order to find the composition range for the new phase, specimens with $x$ values equal to 1, 2, 3 and 5 were synthesized.

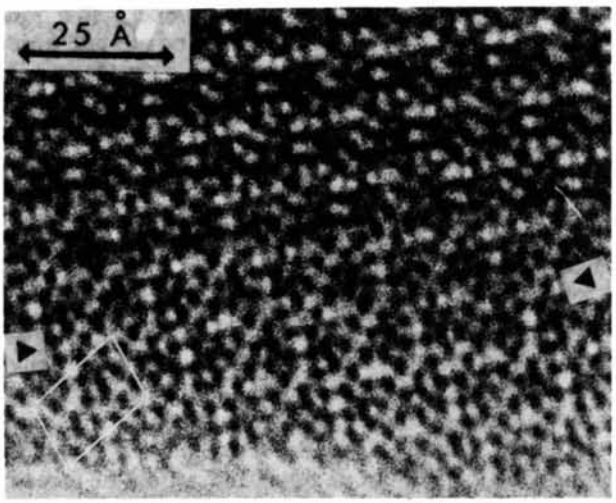


(*a*)

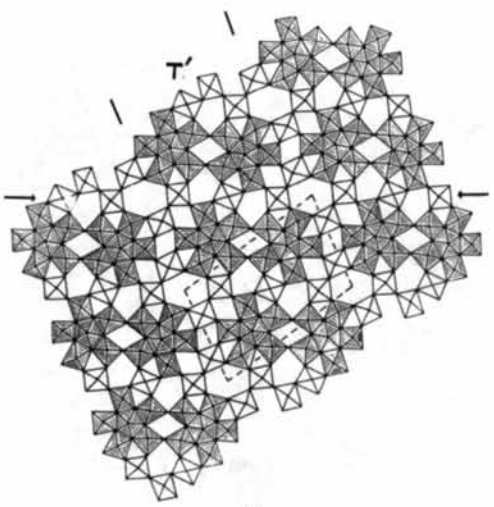


(*b*)

Fig. 1. (*a*) HREM image of the $K_xNb_{8+x}W_{9-x}O_{47}$ ($1 \le x \le 2$) phase along [010] and (*b*) the structure model deduced from the thinnest part of the crystal at the edge in (*a*). A slab one TTB unit cell wide is marked by *T'*. Arrows in (*a*) correspond to those in (*b*).

Table 1. *Atomic coordinates of the structure of* $K_2Nb_{10}W_7O_{47}$

Coordinates were deduced from the (*h*0*l*) projection of the HREM image (Fig. 1*a*). Space group $P2/m$; $Z = 1$; $M$ = Nb,W

| | *x* | *y* | *z* |
|---|---|---|---|
| *M*1 | 0·220 | 0·0 | 0·192 |
| *M*2 | 0·360 | 0·0 | 0·008 |
| *M*3 | 0·552 | 0·0 | 0·220 |
| *M*4 | 0·850 | 0·0 | 0·120 |
| *M*5 | 0·045 | 0·0 | 0·290 |
| *M*6 | 0·690 | 0·0 | 0·495 |
| *M*7 | 0·865 | 0·0 | 0·420 |
| *M*8 | 0·720 | 0·0 | 0·256 |
| *M*9 | 0·500 | 0·0 | 0·500 |
| K1 | 0·382 | 0·5 | 0·270 |
| O1 | 0·220 | 0·5 | 0·192 |
| O2 | 0·360 | 0·5 | 0·010 |
| O3 | 0·560 | 0·5 | 0·220 |
| O4 | 0·850 | 0·5 | 0·120 |
| O5 | 0·045 | 0·5 | 0·290 |
| O6 | 0·680 | 0·5 | 0·502 |
| O7 | 0·860 | 0·5 | 0·420 |
| O8 | 0·720 | 0·5 | 0·256 |
| O9 | 0·500 | 0·5 | 0·500 |
| O10 | 0·160 | 0·0 | 0·030 |
| O11 | 0·118 | 0·0 | 0·210 |
| O12 | 0·304 | 0·0 | 0·140 |
| O13 | 0·255 | 0·0 | 0·340 |
| O14 | 0·450 | 0·0 | 0·100 |
| O15 | 0·497 | 0·0 | 0·340 |
| O16 | 0·394 | 0·0 | 0·440 |
| O17 | 0·102 | 0·0 | 0·430 |
| O18 | 0·950 | 0·0 | 0·380 |
| O19 | 0·625 | 0·0 | 0·140 |
| O20 | 0·635 | 0·0 | 0·340 |
| O21 | 0·740 | 0·0 | 0·100 |
| O22 | 0·813 | 0·0 | 0·270 |
| O23 | 0·760 | 0·0 | 0·420 |
| O24 | 0·957 | 0·0 | 0·160 |

The results showed that the powder photographs taken of samples with $x = 1$ and 2 could be fully accounted for by the new compound, *i.e.* the samples were single phase. The lines could be indexed with a unit cell of monoclinic symmetry with dimensions very similar to those obtained from the electron diffraction pattern. The samples with high potassium content, $x = 3$ and 5, on the other hand, adopted a TTB-related structure, and the Guinier photographs showed diffuse superlattice lines indicating a tripled TTB unit cell, *i.e.* the 3-TTB structure type. However, the least-squares refinement of the unit-cell dimensions was only possible for the subcell. The HREM images also indicated a 3-TTB structure, heavily twinned as usual (Lundberg & Sundberg, 1986). Refined unit-cell parameters and figures of merit for both structure types are given in Table 2.

HREM investigations of the $K_2Nb_{10}W_7O_{47}$ sample showed that most of the examined fragments were well ordered and of the new $M_{17}O_{47}$ structure type. Only a few fragments contained defects or showed intergrowth with a TTB-related structure (see below).

The structure of $K_xNb_{8+x}W_{9-x}O_{47}$ ($1 \le x \le 2$; denoted $K_xM_{17}O_{47}$ below) can be described as built up of slabs of TTB-type structure, one unit cell wide

Table 2. *Unit-cell parameters derived from X-ray powder diffraction data*

E.s.d.'s are given in parentheses. $N$ is the number of lines used in the refinement.

| Compound | $a$ (Å) | $b$(Å) | $c$ (Å) | $\beta$ (°) | $v$ (Å$^3$) | $M(20)^a$ | $F^b$ | $N$ |
|---|---|---|---|---|---|---|---|---|
| $KNb_9W_8O_{47}$ | 18·807 (8) | 3·9450 (9) | 12·333 (5) | 102·88 (5) | 892·01 | 13 | 14 (0·014) | 34 |
| $K_2Nb_{10}W_7O_{47}$ | 18·882 (5) | 3·9572 (5) | 12·378 (2) | 102·93 (3) | 901·41 | 16 | 24 (0·010) | 38 |
| $K_3Nb_{11}W_6O_{47}$ | 12·3351 (5)* | — | 3·9632 (4) | — | 603·02 | 103 | 99 (0·006) | 33 |
| $K_5Nb_{13}W_4O_{47}$ | 12·4192 (6)* | — | 3·9697 (3) | — | 612·27 | 52 | 63 (0·008) | 34 |

References: (*a*) de Wolff (1968), (*b*) Smith & Snyder (1979).

* Calculated for the TTB subcell.

and parallel to the $c$ axis, as marked ($T'$) in Fig. 1(*b*). In the TTB unit cells two out of four five-sided tunnels are filled with $-M-O-M-O-$ strings so that parallel pairs of diamond-linked pentagonal columns (PC's) (Lundberg, Sundberg & Magnéli, 1982; Lundberg, 1971) are obtained. The TTB-type slabs, infinite in two dimensions, are interleaved by additional $MO_6$ octahedra (two per unit cell) through corner sharing; this arrangement produces an ordered array of four- and six-sided tunnels along the $c$ axis which separate the slabs. Note that all pairs of PC's have the same orientation.

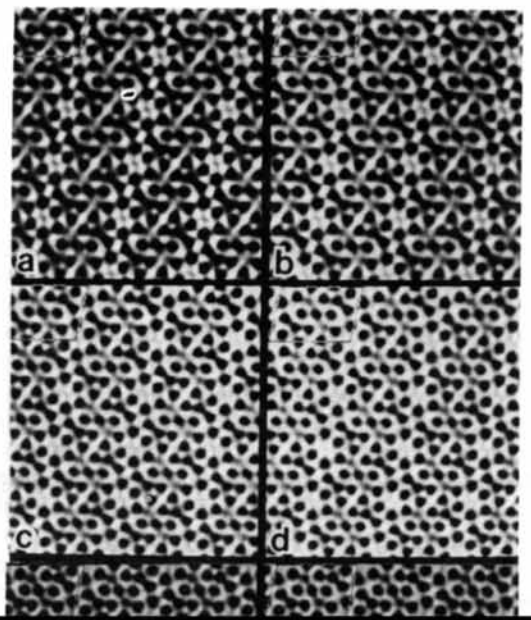


The relationship between the present structure and the well-known tripled TTB-type structure of $Nb_8W_9O_{47}$ (Sleight, 1966) is apparent (see Figs. 1*b* and 3). Fig. 3 shows that the structure of $Nb_8W_9O_{47}$ can be regarded as built up from identical slabs, one TTB unit cell wide as described above, but here alternate slabs occur in twin orientation (they are marked $T$ and $T'$ in Fig. 3), so that an arrangement of five-sided tunnels is formed along the $a$ axis (~12·4 Å), separating the slabs. In the 3-TTB structure there are eight five-sided and six four-sided tunnels available where $A$ atoms can enter the structure. In this case the general formula for the fully oxidized compound will be $A_yNb_{8+y}W_{9-y}O_{47}$, with $0 \le y \le 7$. When $A$ = Na all specimens with values of $y$ within the limits contain TTB-related phases (Hörlin, Marinder & Nygren, 1982). Compounds containing potassium, in contrast, form the 3-TTB structure type only for larger amounts of alkali, while the new structure described above is preferred for low values of $y$ (1 and 2). With $y > 2$ potassium would be forced to enter some of the six- or four-sided tunnels, while in the 3-TTB type structure there are five-sided tunnels

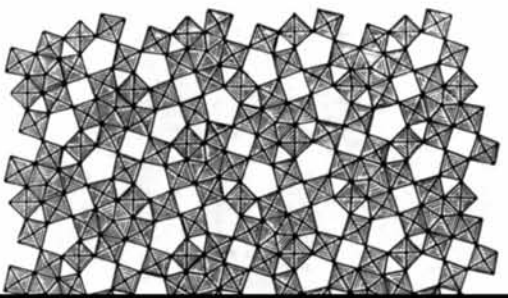

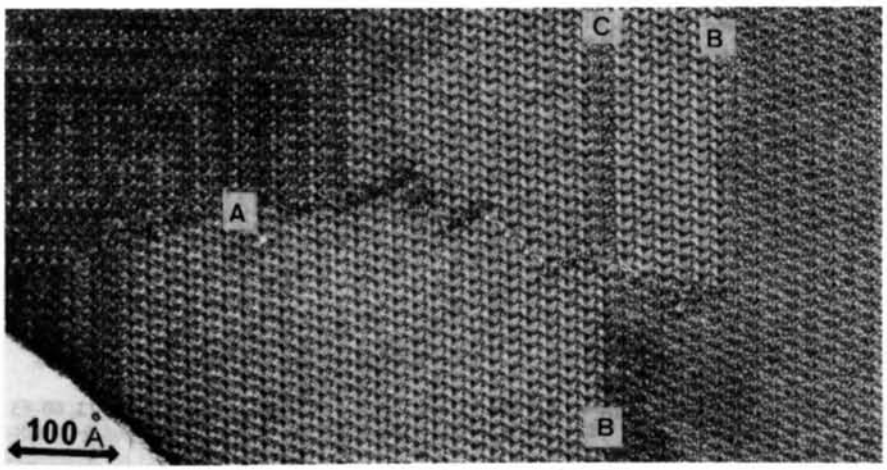


Fig. 4. Low-magnification micrograph of a thin crystal flake of $K_2Nb_{10}W_7O_{47}$. The $Nb_8W_9O_{47}$-type structure to the left, intergrown at *A* with the $K_xM_{17}O_{47}$-type structure ($1 \le x \le 2$). *B* illustrates twinning. *C* shows a 3-TTB intergrowth in the $K_xM_{17}O_{47}$ structure.

available up to $y = 4$. It is known that potassium prefers the five-sided tunnels over the four-sided tunnels in the tetragonal tungsten bronze $K_xWO_3$ (Kihlborg & Klug, 1973). However, the TTB structure also seems to accommodate easily K atoms in the four-sided tunnels (De Pape, Gauthier & Hagenmuller, 1968).

The fact that both structure types may be described as being built up of identical slabs (*T'*) parallel to the 12·4 Å axis makes an intergrowth between these two structures very likely. This has also been observed both in electron diffraction patterns and HREM images and might indicate a slight variation of the K concentration within the crystal. Fig. 4 illustrates an example where a disordered twinned region of the 3-TTB structure type can be seen to the left. At *A* this structure type transforms directly into the $K_xM_{17}O_{47}$ structure, while the latter type occurs in twin orientation to the right. The twin planes are marked *B*. At *C* a slice of the 3-TTB structure type, one unit cell wide, appears as a defect in the $K_xM_{17}O_{47}$ phase. Similarly, the latter structure has previously been observed as a single defect, parallel to the 12·4 Å axis and one unit cell wide, in a micrograph recorded of a flake from a $2Nb_2O_5.5WO_3$ sample with the 3-TTB type lattice (Obayashi & Anderson, 1976).

Fig. 5 illustrates an alternative way of describing the $K_xM_{17}O_{47}$ structure and its relation to $W_{18}O_{49}$ (Magnéli, 1949). Here, the phases are characterized by using the PC–HT–PC (HT = hexagonal tunnel) building block (Fig. 5*a*) (Sahle & Sundberg, 1980). Both structures are built up of roof-tile-stacked, diamond-linked PC–HT–PC groups. In $K_xM_{17}O_{47}$ (Fig. 5*b*) these slabs are linked to each other by direct corner sharing as well as *via* single $MO_6$ octahedra, while in the $W_{18}O_{49}$ structure (Fig. 5*c*) the slabs are mutually joined by edge- and corner-sharing component octahedra as well as by additional pairs of corner-sharing $WO_6$ octahedra. Thus, pairs of diamond-linked PC's are shown in Fig. 5(*b*), while

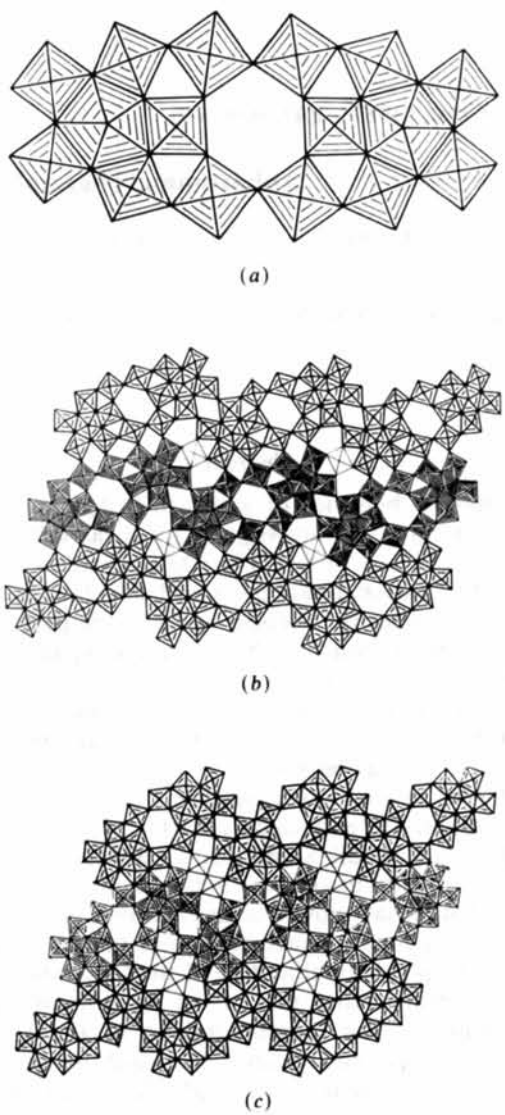


Fig. 5. (*a*) PC–HT–PC, (*b*) the structure of $K_xM_{17}O_{47}$ and (*c*) the structure of $W_{18}O_{49}$ described with PC–HT–PC units.

edge-linked PC pairs can be seen in Fig. 5(*c*). The latter type of PC pairs, however, is the building unit in the $Mo_{17}O_{47}$ structure (Kihlborg, 1960).

We are grateful to Professor Lars Kihlborg for valuable comments on the manuscript and Mrs Gunvor Winlöf for skilful photographic work. This study was supported by the Swedish Natural Science Research Council.

### References

De Pape, R., Gauthier, G. & Hagenmuller, P. (1968). *C. R. Acad. Sci.* **266**, 803-805.
Deschanvres, A., Frey, M., Raveau, B. & Thomazeau, J. (1968). *Bull. Soc. Chim. Fr.* **9**, 3519-3523.
Hörlin, T., Marinder, B.-O. & Nygren, M. (1982). *Rev. Chim. Miner.* **19**, 231-238.
Kihlborg, L. (1960). *Acta Chem. Scand.* **14**, 1612-1622.
Kihlborg, L. & Klug, A. (1973). *Chem. Scr.* **3**, 207-211.
Li, D. Y., Lundberg, M., Werner, P.-E. & Westdahl, M. (1984). *Acta Chem. Scand. Ser. A*, **38**, 813-817.
Lundberg, M. (1971). *Chem. Commun. Univ. Stockholm*, No. XII.
Lundberg, M. & Sundberg, M. (1986). *J. Solid State Chem.* **63**, 216-230.
Lundberg, M., Sundberg, M. & Magnéli, A. (1982). *J. Solid State Chem.* **44**, 32-40.
Magnéli, A. (1949). *Ark. Kemi*, **1**, 223-230.
Obayashi, H. & Anderson, J. S. (1976). *J. Solid State Chem.* **17**, 79-89.
O'Keefe, M., Buseck, P. R. & Iijima, S. (1978). *Nature (London)*, **274**, 322-324.
Sahle, W. & Sundberg, M. (1980). *Chem. Scr.* **16**, 163-168.
Sleight, A. (1966). *Acta Chem. Scand.* **20**, 1102-1112.
Smith, G. S. & Snyder, R. L. (1979). *J. Appl. Cryst.* **12**, 60-65.
Sundberg, M. & Lundberg, M. (1987). *Acta Cryst.* B**43**, 238-244.
Werner, P.-E. (1969). *Ark. Kemi*, **31**, 513-516.
Wolff, P. M. de (1968). *J. Appl. Cryst.* **1**, 108-113.

*Acta Cryst.* (1987). B**43**, 434-440

# Anharmonic Thermal Vibrations in Wurtzite-Type AgI

By Akira Yoshiasa, Kichiro Koto, Fumikazu Kanamaru, Shuichi Emura and Hiroyuki Horiuchi*

*The Institute of Scientific and Industrial Research, Osaka University, Mihoga-oka, Ibaraki, Osaka* 567, *Japan*

(*Received* 16 *January* 1987; *accepted* 20 *May* 1987)

## Abstract

The thermal behavior of atoms in $\beta$-AgI (wurtzite-type structure) was investigated by X-ray diffraction at 123, 297, 363 and 413 K. Determination of the accurate positional parameter and calculation of the probability density function (p.d.f.) were performed by applying a model of the cumulant-expansion up to fourth-order terms. The effective one-particle potentials (o.p.p.) of both Ag and I atoms along the Ag–I bond at each temperature were evaluated from the p.d.f. Several reflections which violate the extra conditions of the systematic absences were observed and explained by anharmonic thermal vibrations. The o.p.p. curves of both atoms disclosed softening of the potentials with increasing temperature. The p.d.f. maps also revealed that the thermal motions of both atoms are strongly anharmonic and that the degree of anisotropic thermal motion of the I atom becomes more prominent than that of the Ag atom at higher temperatures. The thermal motion of the I atom reveals a salient anharmonicity toward the structure transformation from $\beta$- to $\alpha$-AgI. The magnitudes of the temperature factors are larger in mobile Ag atoms than in I atoms. The appreciable anisotropy of the thermal motions is not directly related to the macroscopic characteristics of ionic conduction. Crystal data: $M_r = 234{\cdot}772$, $P6_3mc$, $Z = 2$, Mo $K\alpha$, $\lambda = 0{\cdot}71069$ Å, $\mu = 18{\cdot}14$ mm$^{-1}$, $F(000) = 200$; at 123 K: $a = 4{\cdot}591$ (1), $c = 7{\cdot}511$ (4) Å, $V = 137{\cdot}1$ (1) Å$^3$, $D_x = 5{\cdot}708$ Mg m$^{-3}$, $R = 0{\cdot}023$ for 323 reflections; at 297 K: $a = 4{\cdot}592$ (1), $c = 7{\cdot}510$ (2) Å, $V = 137{\cdot}1$ (1) Å$^3$, $D_x = 5{\cdot}706$ Mg m$^{-3}$, $R = 0{\cdot}029$ for 170 reflections; at 363 K: $a = 4{\cdot}591$ (1), $c = 7{\cdot}508$ (2) Å, $V = 137{\cdot}0$ (1) Å$^3$, $D_x = 5{\cdot}710$ Mg m$^{-3}$, $R = 0{\cdot}020$ for 108 reflections; at 413 K: $a = 4{\cdot}590$ (1), $c = 7{\cdot}506$ (2) Å, $V = 137{\cdot}0$ (1) Å$^3$, $D_x = 5{\cdot}714$ Mg m$^{-3}$, $R = 0{\cdot}017$ for 90 reflections.

## Introduction

The wurtzite-type silver iodide ($\beta$-AgI) shows a considerable ionic conductivity owing to diffusion of Ag ions even at room temperature. It exhibits a negative thermal expansion, and undergoes a first-order phase transition at 420 K to the superionic conducting phase, $\alpha$-AgI, with higher density. The cleavage and gliding perpendicular to the *c* axis occur because of the anisotropy of interatomic force.

* Present address: Mineralogical Institute, Faculty of Science, Tokyo University, Hongo, Tokyo 113, Japan.

0108-7681/87/050434-07$01.50 